Elsevier Editorial System(tm) for Nuclear Inst. and Methods in Physics Research, A
Manuscript Draft

Manuscript Number:

Title: Time-Resolved Data Acquisition for In Situ Subsurface Planetary Geochemistry

Article Type: Research Paper

Section/Category: Special Applications

Keywords: Elemental analysis, pulsed neutron generator, time-tagged data acquisition, optimized time-gating, time-dependent neutron and gamma-ray detection

Corresponding Author: Ms. Julia Gates Bodnarik, M.S.

Corresponding Author's Institution: NASA Goddard Space Flight Center

First Author: Julia Gates Bodnarik, M.S.

Order of Authors: Julia Gates Bodnarik, M.S.; Dan M Burger, B.S.; Arnold Burger, Ph.D.; Larry G Evans, Ph.D.; Ann M Parsons, Ph.D.; Jeffrey S Schweitzer, Ph.D.; Richard D Starr, Ph.D.; Keivan G Stassun, Ph.D.

Abstract: The current gamma-ray/neutron instrumentation development effort at NASA Goddard Space Flight Center aims to extend the use of active pulsed neutron interrogation techniques to probe the subsurface geochemistry of planetary bodies in situ. All previous NASA planetary science missions, that used neutron and/or gamma-ray spectroscopy instruments, have relied on a constant neutron source produced from galactic cosmic rays. One of the distinguishing features of this effort is the inclusion of a high intensity 14.1 MeV pulsed neutron generator synchronized with a custom data acquisition system to time each event relative to the pulse. With usually only one opportunity to collect data, it is difficult to set a priori time-gating windows to obtain the best possible results. Acquiring time-tagged, event-by-event data from nuclear induced reactions provides raw data sets containing channel/energy, and event time for each gamma ray or neutron detected. The resulting data set can be plotted as a function of time or energy using optimized analysis windows after the data are acquired. Time windows can now be chosen to produce energy spectra that yield the most statistically significant and accurate elemental composition results that can be derived from the complete data set. The advantages of post-processing gamma-ray time-tagged event-by-event data in experimental tests using our prototype instrument will be demonstrated.

**Dear NIM-A Editors:**

This cover letter accompanies the submission of the paper: “Time-Resolved Data Acquisition for *In Situ* Subsurface Planetary Geochemistry” for publication in NIM-A.

This paper contains 8 figures and 3 tables. Black and white copies of the figures will be provided for the print version and the enclosed color figures are the web version.

This work has not been published previously in a referred journal and is not under consideration at this time in any other journal.

Possible referees you might wish to consider for this paper are:

1) Dr. William V. Boynton; email: wboynton@lpl.arizona.edu
2) Dr. Russel Hertzog; email: russelhertzog@gmail.com
3) Dr. David Chichester; email: david.chichester@inl.gov

I hope these instructions and the accompanying manuscript and figures are clearly organized and understandable. Please do not hesitate to contact me with questions.

Sincerely,

Julia G. Bodnarik, Corresponding Author
NASA/Goddard Space Flight Center
Solar System Exploration Division
Astrochemistry Laboratory
Code 691
Greenbelt, Maryland 20771

Phone: (301) 286-1398
Mobile: (808) 896-6759
FAX: (301) 286-1683
email: julia.g.bodnarik@nasa.gov; julie.g.bodnarik@gmail.com

# Time-Resolved Data Acquisition for *In Situ* Subsurface Planetary Geochemistry

Author List:

J. G. Bodnarik[a,b*], D. M. Burger[c], A. Burger[d], L. G. Evans[e], A. M. Parsons[a], J. S. Schweitzer[f], R. D. Starr[g], K. G. Stassun[b]

[a]NASA Goddard Space Flight Center, 8800 Greenbelt Rd., Code 691, Greenbelt, MD 20771, USA; e-mail: julia.g.bodnarik@nasa.gov, ann.m.parsons@nasa.gov,

[b]Vanderbilt University, Department of Physics and Astronomy, VU Station B #1807, Nashville, TN 37235, USA; e-mail: keivan.stassun@vanderbilt.edu

[c]Vanderbilt University, VU Station B #351679, 2301 Vanderbilt Place, Nashville, TN 37235-1679, USA; e-mail: dan.burger@vanderbilt.edu

[d]Fisk University, Department of Physics, 240 W.E.B. DuBois Hall, 1000 17th Ave. N., Nashville, TN, 37208, USA; e-mail: aburger@fisk.edu

[e]Computer Sciences Corporation, 7900 Harkins Rd., Lanham, MD 20706, USA; email: larry.g.evans@nasa.gov

[f]University of Connecticut, Department of Physics, Storrs, CT 06269-3046, USA; email: schweitz@phys.uconn.edu

[g]Catholic University of America, Institute for Astrophysics and Computational Sciences, Washington, D.C., 20064, USA; email: richard.d.starr@nasa.gov

[*] Corresponding author. Tel.: provided in cover letter; fax: provided in cover letter; e-mail: julia.g.bodnarik@nasa.gov

**Abstract:**

The current gamma-ray/neutron instrumentation development effort at NASA Goddard Space Flight Center aims to extend the use of active pulsed neutron interrogation techniques to probe the subsurface geochemistry of planetary bodies *in situ*. All previous NASA planetary science missions, that used neutron and/or gamma-ray spectroscopy instruments, have relied on a constant neutron source produced from galactic cosmic rays. One of the distinguishing features of this effort is the inclusion of a high intensity 14.1 MeV pulsed neutron generator synchronized with a custom data acquisition system to time each event relative to the pulse. With usually only one opportunity to collect data, it is difficult to set *a priori* time-gating windows to obtain the best possible results. Acquiring time-tagged, event-by-event data from nuclear induced reactions provides raw data sets containing channel/energy, and event time for each gamma ray or neutron detected. The resulting data set can be plotted as a function of time or energy using optimized analysis windows after the data are acquired. Time windows can now be chosen to produce energy spectra that yield the most statistically significant and accurate elemental composition results that can be derived from the complete data set. The advantages of post-processing gamma-ray time-tagged event-by-event data in experimental tests using our prototype instrument will be demonstrated.

Keywords: Elemental analysis, pulsed neutron generator, time-tagged data acquisition, optimized time-gating, time-dependent neutron and gamma-ray detection

## 1. Introduction

The objective of the current gamma-ray/neutron instrumentation development at NASA Goddard Space Flight Center (GSFC)[1] is to use active pulsed neutron interrogation techniques to determine *in situ* the subsurface bulk elemental concentrations of planetary bodies. To date, all the planetary science missions that have included both neutron and gamma-ray instruments have made remote sensing measurements from orbit or during close fly-by encounters with a planetary body (e.g. Lunar Prospector [1], Mars Odyssey [2,3], Dawn [4], MESSENGER [5], NEAR [6], and LRO [7,8]). The excitation sources for these remote sensing measurements have necessarily been limited to the high energy

[1] Abbreviations:
PNG – Pulsed Neutron Generator
PING – Pulsing In situ with Neutrons and Gamma rays
GSFC – Goddard Space Flight Center
MESSENGER – MErcury Surface, Space ENvironment, GEochemistry and Ranging
LRO – Lunar Reconnaissance Orbiter
NEAR – Near Earth Asteroid Rendezvous
GRC – Galactic Cosmic Rays
MCNPX – Monte Carlo N-Particle eXtended
DSA – Digital Signal Analyzer
PHA – Pulse Height Analysis
TLIST – Time-stamped LIST
HPGe – High Purity Germanium
GGAO – Godddard's Geophysical and Astronomical Observatory

(fast) neutrons that are produced when Galactic Cosmic Rays (GCR) interact with planetary materials. Although GCR-generated fast neutron rates change with the 11-year solar cycle, they occur at a constant rate for these measurements time. Measured gamma-ray spectra contain all of the gamma ray lines from each of the gamma ray-producing interactions of neutrons with the planetary material. Gamma-ray spectra thus include peaks resulting from inelastic scattering, thermal neutron capture, delayed activation and natural radioactivity. However, the large number of peaks and the high spectral background result in peak interferences, misidentifications and reduced precision in the reported gamma-ray results. These difficulties are avoided for *in situ* measurements of a landed instrument package that includes a Pulsed Neutron Generator (PNG) as the excitation source. A PNG can produce fast neutrons at ~100 times greater rate than GCR interactions resulting in significantly reduced measurement times for equivalent sensitivity. A PNG can also produce 14.1 MeV neutrons in relatively short bursts with an adjustable neutron pulse period and width. With the production of the high-energy neutrons restricted to the duration of the burst, the gamma rays that result from the inelastic scattering of these fast neutrons will also occur only during the time of the burst. Between each burst, the planetary material moderates the fast neutrons so that the gamma rays are largely produced by thermal neutron capture. After most of the thermal neutrons have been absorbed, the gamma rays resulting from delayed activation and natural radioactivity become visible. Separating the gamma rays by their detection time relative to a PNG pulse results in lower background and a

substantial reduction in peak interferences, while capturing essentially all of the gamma rays due to a particular type of reaction. Separating gamma ray spectra by physical process minimizes the systematic effects from interfering peaks and provides improved precision and accuracy in the peak analysis that directly results in more precise elemental concentration measurements. We have previously shown [9] that significant improvements in precision can be obtained using properly chosen time windows for time-gated coincidence data acquisition methods. Here we report the increased benefits of using time tagged event-by-event data.

On Earth, it is possible to adjust the PNG pulse period and width as well as the coincident data acquisition window timing parameters for an optimum analysis of a sample because one usually has a general idea of the sample's bulk composition and its properties with regard to neutron and gamma ray transport. Even without this knowledge, multiple measurements using adjusted parameters are usually possible. So it is often simple and sufficient to use coincidence data acquisition methods with a limited number of fixed time gates for these ground-based experiments on Earth. However, one rarely has the luxury of repeating measurements on another planet. When making *in situ* measurements on a planetary body, there is often a great ignorance of its composition especially with regard to elements that affect the neutron and gamma ray time dependence. For planetary science applications it would be very difficult to make multiple measurements at a variety of different timing conditions with sufficient statistics to determine the optimum timing parameters. The optimal timing parameters

largely depend on neutron transport properties that are governed by effects that vary by location such as elemental composition, hydrogen content, density and subsurface layering geometries. By the time one has determined what the proper time gating should be, the mission may be over, or, in the case of a rover mission, the rover may have already left the region where the earlier data were obtained.

This type of problem has been addressed in early NASA Apollo gamma ray experiments [10] as well as in other scientific fields such as radioanalytical chemistry applications [11] by accumulating data on an event-by-event basis where the energy and measurement time is recorded for every event detected during the data acquisition time. When data are accumulated in an event-by-event mode that includes event times, one can analyze the data after the measurement has been made (post-processing) to determine the optimum time windows for spectral data analysis. Although event-by-event data acquisition leads to large raw data files, it makes it possible to perform the optimal spectral analysis without requiring repeated measurements.

### *1.1 The Probing In situ with Neutrons and Gamma rays (PING) Instrument*

Our group at NASA/GSFC is currently developing the Probing *In situ* with Neutrons and Gamma rays (PING) instrument for planetary *in situ* bulk elemental composition measurements [9] by leveraging both well-established oil well and scientific logging techniques [12] and remote sensing planetary gamma-ray spectroscopy techniques. PING employs a 14.1 MeV pulsed neutron generator to excite materials at and below a planetary surface and utilizes the penetrating

nature of these fast neutrons and gamma rays to probe the subsurface soil composition over a 1 $m^2$ area and down to depths of 10-100 cm. PING's gamma-ray spectrometer and neutron detectors measure the resulting gamma rays and neutrons that emerge from the planetary surface. To illustrate an example application, PING is shown in Figure 1 attached to the underside of a planetary rover.

< Insert Figure 1>

A gamma-ray spectrometer measures the resulting inelastic scattering, capture, and delayed activation gamma rays emitted by the excited elements as well as gamma rays emitted from natural radioactive decay; neutron detectors measure the number of the epithermal and thermal neutrons that reach the surface as a function of time relative to the initiation of each high-energy neutron pulse. PING gamma-ray and neutron data are acquired using custom software to control digital signal analyzer electronics. These data, coupled with MCNPX [13] computer simulations, let us quantitatively determine the bulk elemental composition of the subsurface material for any solid body in the Solar System, even bodies with a dense atmosphere. PING can measure a wide range of elements (e.g. C, H, O, P, S, Si, Na, Ca, Ti, Fe, Al, Cl, Mg, Mn, K, Th, and U) depending on their abundance in the planetary material.

*1.2 Outdoor Neutron-Gamma Ray Instrument Test Site*

We are testing the capabilities of our PING instrument prototypes at a unique outdoor gamma ray and neutron instrumentation testing facility located at Goddard's Geophysical and Astronomical Observatory (GGAO) near Goddard's

main campus. A schematic view of the test site is shown in Figure 2. This test facility allows us to operate PING on top of either of two large, well-characterized granite and basalt monuments, each 1.8 m x 1.8 m x 0.9 m in size. Activation Laboratories Ltd. in Ancaster, Ontario, Canada, has independently measured the full elemental compositions of these Concord Gray Granite and Columbia River Basalt materials to the ppm level. PING is remotely operated from a building more than 75 m from the monuments due to the radiation hazard from the PNG's 14 MeV neutrons. Underground power and communications lines connect the operations building to the test monuments. Details of the specific PING measurements are given in Section 3.1 and further information about the test facility can be found in [14,15].

< Insert Figure 2>

*1.3 Using TLIST Data to Improve PING Elemental Composition Measurements*

A Canberra Lynx Digital Signal Analyzer (DSA) is used to acquire data from each gamma ray and neutron detector used for a PING measurement. While the Lynx DSA hardware [16], features multiple data acquisition modes, including coincidence-gated Pulse Height Analysis (PHA) and event-by-event Time-stamped LIST (TLIST) mode, operation of the Lynx DSAs in TLIST mode required the development of custom software. In this paper, we describe both the acquisition of TLIST data using our custom MultiScan software [17] and the post-processing of our data that allows us to:

1) Use optimized timing windows to separate the data into distinct gamma-ray spectra resulting from either a) inelastic scattering, during the neutron

pulse, b) thermal neutron capture, between neutron pulses, or c) delayed activation and natural activity events visible just before the next fast neutron pulse. This separation allows us to more accurately identify gamma ray lines and more precisely measure gamma ray net peak areas;

2) Isolate a particular energy line from a gamma ray spectrum and observe its intensity time profile with respect to the PNG pulse to more accurately identify and measure the gamma-ray line and its net peak area; and

3) Extract gamma ray data to optimize the timing windows needed to look for specific elements in different environments and to obtain the optimum precision for the analyzed peak intensities.

## 2. The TLIST Data Acquisition Technique

Analyzing individual gamma-ray peaks in a traditional PHA energy spectrum can be challenging due to both interfering lines and the background continuum resulting from multiple processes. We reduce these effects and obtain higher gamma-ray line sensitivity with increased signal-to-noise by recording gamma-ray time and energy in an event-by-event mode. We use our custom MultiScan software and the Canberra Lynx DSA in TLIST mode to record the energy and time (temporal resolution 0.1 μs) of each event detected during a PNG pulse cycle. As discussed in Section 1, we obtain a master data set that is not limited to predetermined coincidence timing gates set for specific nuclear processes. This master data set can be sliced in many ways without loss of information or requiring additional measurements with different data acquisition window settings.

Figures 3a and b illustrate the results of our post-processing of TLIST gamma-ray data for various timing windows.

< Insert Figures 3a and 3b>

Figure 3a is an illustration of the PNG fast neutron pulse train and the intra-pulse location of the different timing windows needed to separate the gamma rays that result from the inelastic scattering, thermal neutron capture, delayed activation and natural radioactivity processes. Figure 3b is an illustration of the differences in the resulting energy and intensity of the gamma ray lines and background for each of these separated spectra.

*2.1 Custom MultiScan Data Acquisition Software*

Lynx DSA data acquisition can be performed using either the Lynx web-based interface or the Genie 2000 software package [16] both available from Canberra Industries. Although the Lynx DSA hardware offers the required TLIST mode, neither of these software options provides the flexibility and all of the capabilities we need for our specific instrument application. The MultiScan software, designed specifically for our project, allows us to 1) acquire data in TLIST mode while synchronized to the PNG pulse, 2) save data in ASCII format, 3) analyze TLIST data for an unlimited number of time windows, and 4) perform multiple consecutive data acquisitions while maintaining the Lynx graphical analysis and configuration features. Example images of the MultiScan software interface are shown in Figure 4.

< Insert Figure 4>

The MultiScan software was written in Java, since we needed to make the code cross-platform and easy to understand so that others can make changes to the code when necessary. When starting a new data acquisition or scan, the user can specify which of the multiple Lynx DSAs to perform the scan, the acquisition mode (PHA or TLIST), the file format to save the data (Canberra CNF file, ASCII text, or both), how many consecutive scans to perform, and the duration of each scan (in either live time or true time). Settings can be modified quickly and easily within the software. The data are both written to a file and presented in a large display window with multiple data visualization features. The program also provides basic data analysis tools for both PHA and TLIST scans, and off-line TLIST data post-processing time-slicing tools, as well as a diagnostic feature for monitoring the operating parameters within the Lynx DSA [18].

### *2.2 TLIST Data Analysis Techniques*

We use the MultiScan software with Lynx DSAs to acquire TLIST data for gamma-ray and neutron detectors with the start of a data acquisition synchronized with the start of a PNG pulse. Synchronization of the PNG and DSA clocks insures the accuracy of these event times over multi-hour data acquisition runs. Our basic post-processing procedure for the individual event-by-event data files is to take the modulus of the absolute times for the detected events with respect to the known PNG pulse period to derive the time of each event relative to the neutron pulse. The next step is to put all of the files for a given experiment on the same time base. The result is a master data set of energies and relative event times that can be “sliced” in any number of ways.

241 Slicing the data in time means establishing the boundary between times where
242 different nuclear processes dominate. The result is separate gamma-ray spectra
243 for the specific processes that have the event statistics characteristic of the total
244 acquisition time. Slicing the data in energy means establishing energy
245 boundaries around spectral features whose time profile one wishes to study.
246 After generating this master data set with energy and relative time values, we
247 can analyze our gamma ray and neutron data to infer the bulk elemental
248 composition, density, and subsurface layering of planetary bodies.

249 **3. Experiments and Results with TLIST Data**

250 Gamma-ray and neutron spectroscopy is used to infer the bulk elemental
251 concentrations of the surface and subsurface of planetary bodies. The time
252 dependence relative to the neutron burst of gamma ray peaks in an energy
253 calibrated spectrum can be analyzed to determine the neutron-nuclei
254 interaction(s) associated with a particular gamma ray energy. We performed
255 PING experiments using a pulsed neutron generator, gamma ray and neutron
256 detectors on a meter-sized basalt monument. The TLIST data acquired and
257 analyzed in this section only represents 6.33 hours of data acquisition with a
258 fixed neutron pulse with a width of 100 μs and a pulse period of 1000 μs. The
259 results of TLIST data acquisition and post-processing presented will demonstrate
260 the improved precision and reduced systematic errors that can be achieved as
261 compared with pre-assigned acquisition windows from a presumed knowledge of
262 elemental composition.

263 *3.1 Experiment Description*

During these experiments, we acquired 6.33-hrs of TLIST data using a Lynx DSA connected to an n-type Ortec GMX Series HPGe portable coaxial detector system and a 14 MeV Deuterium - Tritium Thermo Fisher MP320 portable PNG [19] positioned on top of our Columbia River basalt monument, as shown in Figure 5.

< Insert Figure 5>

The Lynx DSA reading out the HPGe detector was connected directly to the PNG to synchronize the start of each data acquisition run with the start of a neutron pulse. The PNG beam current, high voltage, frequency, and duty factor were set to 60 μA, 50 kV, 1 kHz, and 10% respectively. At these settings, the PNG produced a neutron pulse width, pulse period, energy, and rate of 100 μs, 1000 μs, 14 MeV, and 3 x $10^7$ n/s respectively.

*3.2 Gamma-Ray Peak Separation Using TLIST Data Analysis*

Gamma-ray line identification can be difficult for many reasons including: 1) interfering gamma-ray lines resulting from the use of low energy resolution gamma-ray spectrometers (i.e. NaI gamma ray scintillation detectors); and 2) multi-element neutron-nuclei interactions that produce gamma rays at the same energy that are indistinguishable even when using high energy resolution gamma-ray spectrometers (e.g. HPGe semi-conductor detectors). Unfortunately, it is difficult to deal with these gamma-ray line identification problems when analyzing gamma-ray remote sensing data, because remote sensing gamma-ray spectroscopy is limited by the collection of PHA energy spectra and the use of the constant neutron source resulting from GCR interactions with the planet.

However, these gamma-ray line identification problems can be easily addressed with the PING instrument by taking advantage of the pulsed nature of the *in situ* neutron source synchronized with the data acquisition system.

Figure 6 shows an example of interfering lines common in gamma-ray PHA energy spectra collected by low energy resolution detectors. Here we see two interfering lines in a gamma-ray spectrum taken using the PING instrument with a $LaBr_3$ scintillation detector on top of a granite and polyethylene configuration.

<Insert Figure 6>

The counts in the unresolved peak area are primarily from $^{28}Si$ and $^{56}Fe$ gamma rays. The natural solution would be to use a gamma-ray spectrometer with better energy resolution, but one does not always have that option due to mass, power, volume and cost constraints associated with planetary space flight missions. One way to remedy this problem is to separate the gamma-ray energy spectra by nuclear process using the gamma-ray event times as shown in Figure 7.

<Insert Figure 7>

Figure 7 is a plot of four different gamma-ray PHA spectra, with the lines from Table 1 indicated, for a 6.33-hr live time acquisition with the PING instrument using a HPGe detector on the basalt monument, consisting of: 1) a total gamma-ray spectrum (in black) including all neutron-nuclei gamma-ray processes; 2) an inelastic gamma-ray spectrum (in red) created by only selecting gamma-ray events during the PNG pulse for t=20-100 μs; 3) a neutron capture gamma-ray spectrum (in green) created by only selecting gamma-ray events after the PNG pulse for t=150-650 μs; and 4) a delayed activation and natural activity gamma-

ray spectrum (in purple) created by only selecting gamma ray events for t=650-999 μs. Separating the gamma-ray acquisition into different time slices allows us to isolate gamma-ray events for specific interactions from a single element without accumulating excessive background when the peaks are not actually present.

<Insert Table 1>

Even if a better energy resolution detector like HPGe is used, gamma-ray line identification can still be challenging, due to multi-element neutron-nuclei interactions that produce gamma rays at the same energy but from different elements. For example, Table 2 lists a selected set of gamma-ray line energies and their possible sources from neutron-nuclei interactions with different elements, demonstrating how multiple elements can contribute to the same line energy.

<Insert Table 2>

Problems with interfering lines can be dealt with by examining the time profile of the individual gamma ray lines. Figure 8a is an example of a 6.33-hr summed HPGe gamma ray spectrum taken with PING instrument on top of the basalt monument. In this spectrum, the Doppler broadened $^{27}Al(n,n'\gamma)$ gamma ray line from neutron inelastic scattering, the $^{1}H(n,\gamma)$ gamma ray line from neutron capture, and the $^{24}Na(n,\beta\gamma)$ SE from delayed activation are clearly interfering with one another. One way to distinguish $^{27}Al(n,n'\gamma)$ and the $^{1}H(n,\gamma)$ gamma ray lines is by plotting the net peak area of the unresolved spectral feature in Figure 8a as a function of time, as shown in Figure 8b, to distinguish which line is present.

Figure 8b shows the time histograms of the net peak areas for the 2211 keV $^{27}$Al(n,n'$\gamma$) and the 2223 keV $^{1}$H(n,$\gamma$) gamma ray lines. The time histograms are the gamma-ray count rates per 10 μs time interval and demonstrate that one can distinguish between and separate interfering lines by nuclear process to improve both the peak identification and the measurement precision.

< Insert Figures 8a and 8b>

*3.3 Improved Gamma-Ray Measurement Precision*

Separating a gamma-ray spectrum by nuclear process improves the overall gamma-ray line measurement precision. As seen in Table 1 in Section 3.2 many of the time-gated inelastic scattering and capture lines show improved precision as compared with the same lines in the summed spectrum. The 3539 and 4934 keV $^{28}$Si(n,$\gamma$) capture lines show improved precision resulting from time-gated analysis. The precision of these Si lines in the summed spectrum, representing results without time slicing, is 8.3% and 16.92%. These same Si lines show improved precision (7.3% and 9.21%) in the capture-delayed activation spectrum obtained with optimized time gating from the removal of the gamma-ray background due to inelastic scattering. A similar but somewhat smaller improvement is seen for the 2211 keV $^{27}$Al(n,n'$\gamma$) inelastic line.

An interesting situation is observed for the 1779 keV $^{28}$Si(n,n'$\gamma$) and 6129 keV $^{16}$O(n,n'$\gamma$) inelastic lines shown in Table 1. These gamma rays are also produced in the other two spectra by delayed activation reactions (see Table 2). Therefore, the 1779 and 6129 keV gamma ray lines in the summed spectrum have a better statistical precision of 0.48% and 1.10% as compared to 1.00% and 1.67%

(inelastic spectrum) and 0.52% and 1.42% (capture-delayed activation spectrum), because there are more counts in the summed spectrum.

The 1779 and 6129 keV lines are not as useful for determining elemental weight percent, because they have a large contribution due to delayed activation. However, the data in the capture-delayed activation spectrum can be used to correct the data in the inelastic spectrum for the portion of the counts that are due to inelastic scattering. While this correction leads to a deterioration of the statistical precision of the weight percent determination from the inelastic data, it provides elemental concentrations that have dramatically improved accuracy.

*3.4 Identifying and Removing Sources of Systematic Error Using TLIST data*

Space-based planetary science missions are unique, because there is usually only one opportunity to collect data. Gamma ray and neutron spectroscopy remote sensing measurements are further restricted to only gamma rays or neutrons produced by a constant neutron flux source created by GCR interactions with the planetary surface and atmosphere. With a weak constant neutron source there is no need to record event-by-event time and energy data if the data are transferred periodically with reasonable frequency, since each chunk of transferred data can be separately analyzed to identify a problem with the instrument, e.g. deteriorated resolution, and removed without compromising the entire concatenated data set. However, it is still difficult to determine if the collected data have been compromised due to other errors. These difficulties can be mitigated for the case of *in situ* gamma-ray and neutron spectroscopy measurements with the PING instrument, since it takes advantage of a pulsed

neutron generator synchronized with gamma ray and neutron detector data acquisition combined with the ability to post-process acquired time-tagged event-by-event data.

A unique benefit of incorporating a pulsed neutron generator with a time-tagged event-by-event data acquisition system is that regions in time containing suspicious data can be isolated and removed from the data set for further inspection without affecting the usefulness of the remaining data. Systematic errors in data are nearly impossible to anticipate but often can be identified when examining the post-processed data. Examples include systematic errors caused by equipment operating parameter changes, such as temperature effects on a detector response or, as illustrated in the data shown in Table 3 below, changes in the time-dependence of the turn on of neutron-induced gamma-ray flux that occurs during the PNG burst period.

< Insert Table 3>

We demonstrate the merit of saving event-by-event time and energy data with our analysis of the gamma-ray count rate of the 6129 keV peak from neutron inelastic scattering on $^{16}O$ for a 2-hr live time gamma-ray acquisition by the PING instrument set-up on the basalt monument. Since the neutron inelastic scattering gamma-ray production rate is proportional to the fast neutron flux, we assume that a stable gamma-ray count rate can be obtained from the time the “pulse start” signal is given to the PNG ion source (t = 0 $\mu$sec). We can examine the time dependence of the fast neutron-induced gamma-ray flux from the time of the

401 “pulse start” signal to the end of the PNG pulse (t = 0 to 100 μsec) to look for
402 anomalies.
403 In this example, we generated gamma-ray energy spectra for each of ten time
404 slices (time slice width = 10 μsec) of the gamma-ray data during the PNG pulse
405 and determined the 6129 keV net gamma-ray peak count rate and its associated
406 uncertainty for each time slice. Table 3 lists the time range for each time slice,
407 the 6129 keV peak count rates and the uncertainty in the count rates for each of
408 the ten time slices. Note that the count rates in the first and second time slices
409 are inconsistent with the count rates in the 8 other time slices and that the count
410 rate for these later 8 time slices is constant as expected.
411 The low 6129 keV gamma-ray count rate during the first time slice (t = 0-10
412 microseconds) indicates that the PNG has not begun producing fast neutrons yet,
413 since there is a delay between the time that the PNG is sent the “burst on”
414 command signal and the time when fast neutrons are actually being generated
415 by the PNG. The higher 6129 keV gamma-ray count rate in the second time
416 slice (t = 10-20 microseconds) is also inconsistent with the average value for the
417 other slices and may be due to a systematic error induced by the gamma-ray
418 detector electronics. In both cases, we can choose to exclude these data points
419 from further analysis, since they are not representative of the constant inelastic
420 gamma-ray flux during the PNG pulse.
421 To be sure, we would investigate the origin of the systematic errors that
422 prompt us to remove the data from the main analysis. Without this event-by-
423 event time and energy data, however, these points would have been unexamined

and included in the data, skewing the results. Excluding the data from the first 20 μs will increase the statistical error on the mean value of the 6129 keV gamma-ray production rate, but will result in more accurate data that we can use to infer the bulk elemental composition of planetary material. This is clearly seen by comparing the 6129 keV weighted mean count rate and uncertainty for time slices 3 through 10 (t = 20 -100 μs) which is 42.2 cts/μs ± 1.10 cts/μs versus the 6129 keV weighted mean count rate and uncertainty for time slices 1 through 10 (t = 0 -100 μs) which is 30.1 cts/μs ± 0.82 cts/μs. The difference between these two averages is almost ten times the statistical uncertainty, resulting in a very significant systematic error that would compromise the accuracy of derived elemental concentrations.

## 4. Conclusions

Many of the problems typically encountered by planetary gamma-ray elemental composition measurements are addressed by using PING in event-by-event data acquisition mode. For example, it is generally impossible to know *a priori* how to set optimum time windows for gamma-ray detection when using a pulsed neutron generator as the source of neutrons, because of compositional variations from location to location on a planetary body. This is a real problem because there is usually only one opportunity to acquire a specific set of data during planetary missions. This problem is solved when taking data in an event-by-event mode, because data can be analyzed after it is collected and therefore set optimum time windows based on the data.

Our goal is to obtain the best estimate of elemental concentrations from the gamma-ray data. However, the same energy gamma ray can often be created from different isotopes via two different reaction mechanisms. In such instances we can separate out different time regions where a particular gamma ray is due to a specific reaction mechanism.

Post-processing event-by-event data allows PING to obtain the best precision and most accurate results. For example, in the analysis of a peak that only occurs in one time region, one can reduce its uncertainty by ~40% by eliminating background in that energy region that occurs at times when the peak is not present. Perhaps even more important is the improvement in accuracy that can be achieved when the same gamma ray peak can be obtained at different times from different reaction mechanisms. The inelastic window in Table 1 for the 1779 gamma-ray peak is largely from the $^{28}$Si(n,n'$\gamma$) reaction. However this area must be corrected for the delayed activity present. The result is a factor of 3 smaller than the 1779 keV area for the entire time spectrum, but the reduced area can now be converted to weight percent Si.

Another improvement in the accuracy of the results can be obtained by eliminating data when it appears the instrument is not performing properly as shown in Table 3 and discussed in Section 3.4. For example, the 6129 keV weighted mean average for 0-100 $\mu$s is 30.1 cts/$\mu$s ± 0.82 cts/$\mu$s and for 20-100 $\mu$s is 42.2 cts/$\mu$s ± 1.10 cts/$\mu$s. Although the statistical error of the weighted mean average increases when you exclude the first 20 $\mu$s, the difference between these two averages is almost ten times the statistical uncertainty and

would significantly impact the accuracy of the derived bulk elemental concentrations of planetary material.

We can also minimize instrumental problems by subdividing the total data set at certain times to investigate such things as gain shifts. Thus by independently analyzing subsets of the data, you can preserve data quality that would be compromised if you where limited to only analyzing PHA data.

When using a pulsed neutron source, the potential exists for obtaining higher precision data. By using event-by-event data acquisition, the risk of improper timing settings is eliminated and systematic errors can be reduced or eliminated. Taken together, event-by-event data acquisition of pulsed neutron-induced gamma ray spectra for determining elemental concentrations, provides significant enhancements to measurements obtained on a planetary surface resulting in the best scientific information on a particular mission.

**Acknowledgements**

We would like to thank S.L. Floyd, M. Namkung, and S.F. Nowicki for assistance with acquiring the data. We would like to thank R. Forsythe for assistance with the data analysis. We would like to thank J.I. Trombka and T.P. McClanahan for many useful discussions. We are indebted to NASA, NSF, and the Tennessee Space Grant for partial support of this research.

## References


[1] W.C. Feldman, et al., J. Geophys. Res. 109 (2004) E07S06.

[2] W.V. Boynton, et al., Space Sci. Rev. 110 (2004) 37.

[3] W.V. Boynton, et al., Science 297 (2002) 81.

[4] T.H. Prettyman, et al., IEEE Trans. Nucl. Sci. N50 (2003) 1190.

[5] J.O. Goldsten, et al., Space Sci. Rev. 131 (2007) 339.

[6] L.G. Evans, et al., MAPS 36 (2001) 1639.

[7] I.G. Mitrofanov, et al., Space Sci. Rev. 150 (2010) 183.

[8] I.G. Mitrofanov, et al., Astrobiology 8 (2008) 793.

[9] A. Parsons, et al., Nucl. Instr. and Meth. A 652 (2011) 674.

[10] A.E. Metzger, et al., Science 179 (1973) 800.

[11] L. Szentmiklosi, et al., J. Radioanal. Nucl. Chem. 262 (2005) 213.

[12] J.A. Grau, et al., IRRMA '92, Raleigh, NC, 8-11 Sept., 1992; Int. J. Rad. Appl. Instr. Part E, 7 (1993) 173.

[13] D.B. Pelowitz, et al., (2005) MNCPX User's Manual, Version 2.5.0, LANL, Los Alamos, LA- UR-05-0369.

[14] J. Bodnarik, et al., 41st LPSC, Woodlands, TX, 1-5 Mar., 2010; Conf. Proc. 41 (2010) 2581.

[15] P. Ann, et al., 2011 IEEE (NSS/MIC), Valencia, Spain, 23-29 Oct., 2011; IEEE Conf. Rec. (2011) 1234, doi: 10.1109/NSSMIC.2011.6154608.

[16] CANBERRA Lynx Digital Signal Analyzer application note (2012) http://www.canberra.com/literature/438222.asp.

[17] J.G. Bodnarik, et al., 2010 IEEE (NSS/MIC), Knoxville, TN, 30 Oct. – 6 Nov., 2010; IEEE Conf. Rec. (2010) 1, doi: 10.1109/NSSMIC.2010.6036247.

[18] D. Burger, personal communication, 2011.

[19] D.L. Chichester, et al., J. Radioanal. Nucl. Chem. 271 (2007) 629.

## Figure Captions and Titles

**Figure 1. Illustration of PING**. The instrument is mounted on the underside of a planetary surface rover. Also shown are the different nuclear processes that produce the gamma rays and scattered neutrons that are detected at the surface.

**Figure 2. Aerial view of GGAO.** This schematic of the outdoor gamma ray and neutron instrumentation testing facility shows the operations control building as well as the 46 m diameter safety perimeter surrounding the two existing 1.8 m x 1.8 m x 0.9 m granite and basalt monuments.

**Figures 3. Timing Windows and Sample Spectra.** a) Placement of timing windows relative to each PNG pulse. b) Examples of different spectral shapes seen in different timing windows.

**Figure 4. Images of MultiScan Screens**. MultiScan was written using the Java programming language, the NetBeans integrated development environment (IDE), and the Lynx software development kit (SDK).

**Figure 5. PING Experiment Set-up.** PING deployed for measurements on top of the basalt monument. The PNG is on the left, the HPGe detector is on the right, and $^{3}$He detectors are between them. The data acquisition electronics are situated behind the basalt and are not visible in this photo.

**Figure 6. $LaBr_3$ Spectrum.** An example of unresolved lines in a portion of a gamma ray spectrum taken using the PING instrument with a $LaBr_3$ scintillation detector on top of a granite and polyethylene configuration.

**Figure 7. Spectra from Different Time Windows.** Gamma-ray spectra from a 6.33-hr acquisition using a HPGe detector on top of Columbia River basalt.

**Figure 8. Spectral Feature and Time Distribution.** a) A portion of the non-time sliced 6.33-hr gamma ray energy histogram from PING data taken on the bare basalt monument. b) Time histogram showing how one can get better precision on the net peak area of each line, shown in Table 1, by analyzing their respective energy histograms during different time slices during the PNG pulse period.

**Table Captions**

566

567 Table 1. HPGe gamma-ray line intensities (Ig) and uncertainties (s) for a 6.33-hr

568 PING acquisition on the bare Columbia River basalt monument.

569

570 Table 2: $\gamma$-ray lines to analyze for inelastic $\gamma$-ray spectra time window

571 optimization.

572

573 Table 3. Fast neutron induced count rate and uncertainty for the 6129 keV

574 $^{16}O(n,n'\gamma)$ gamma ray peak for ten time slices during the PNG pulse.

# Figure(s) 1

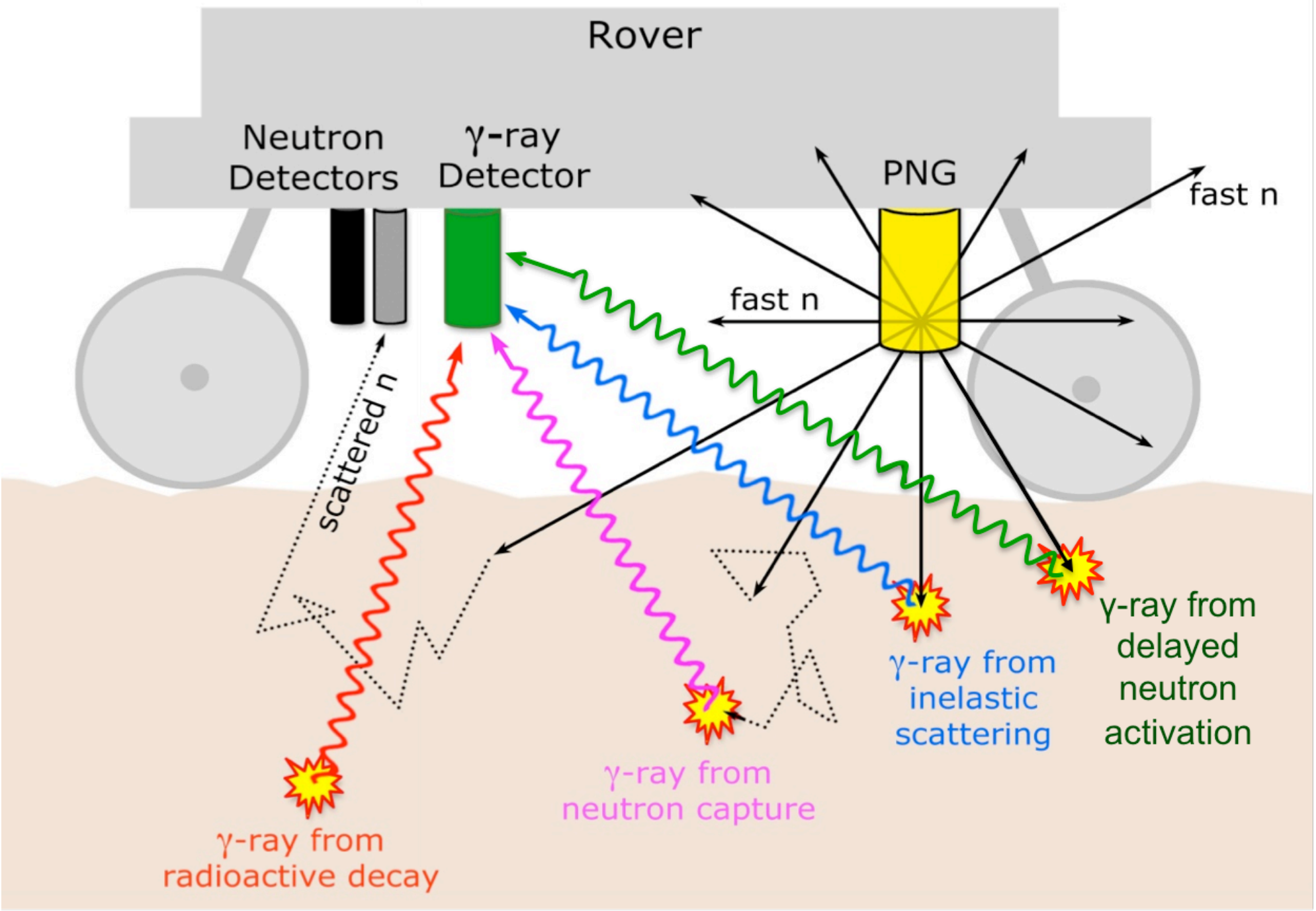
Rover
Neutron Detectors
γ-ray Detector
PNG
fast n
fast n
scattered n
γ-ray from radioactive decay
γ-ray from neutron capture
γ-ray from inelastic scattering
γ-ray from delayed neutron activation

Figure(s) 2

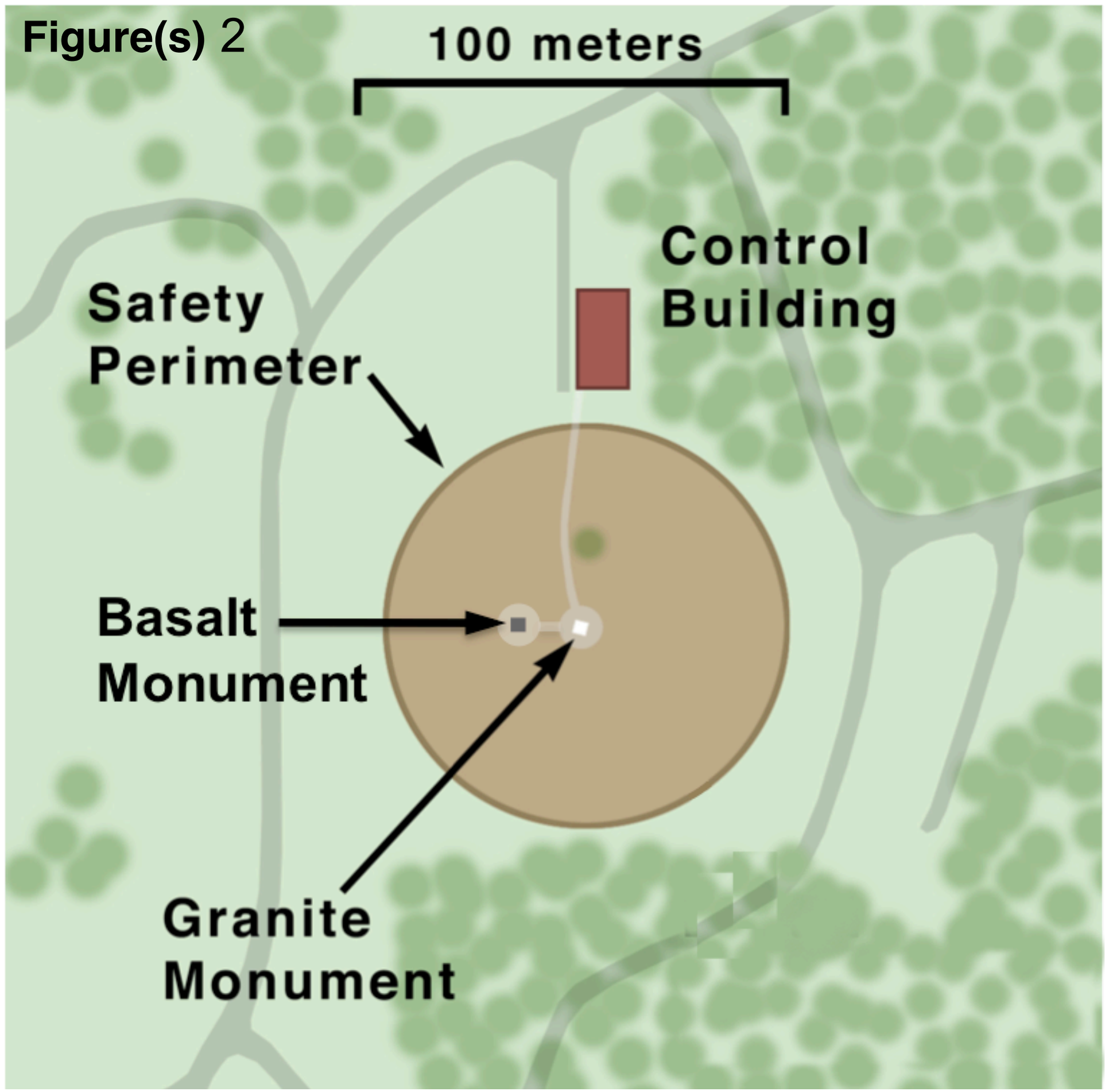
100 meters
Control Building
Safety Perimeter
Basalt Monument
Granite Monument

**Figure(s)** 3

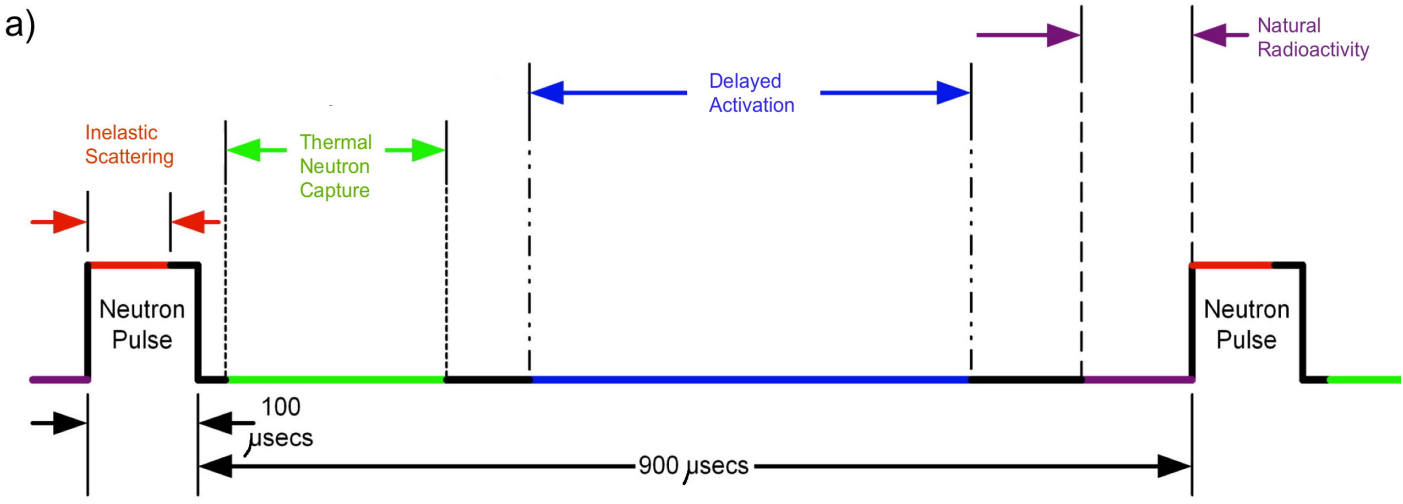
a)
Natural
Radioactivity
Delayed
Activation
Inelastic
Scattering
Thermal
Neutron
Capture
Neutron
Pulse
Neutron
Pulse
100
μsecs
900 μsecs

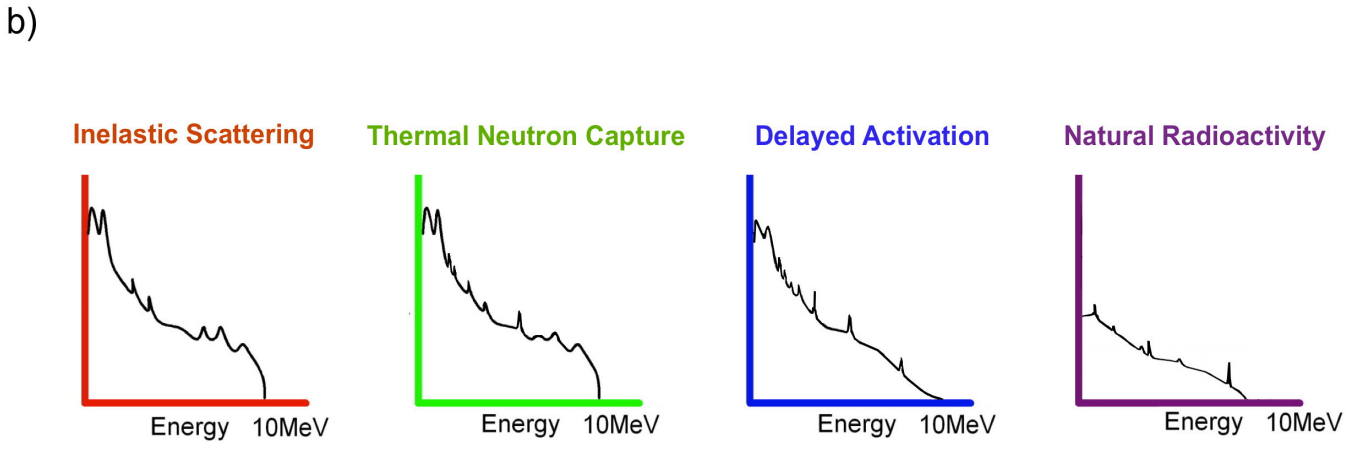
b)
Inelastic Scattering
Thermal Neutron Capture
Delayed Activation
Natural Radioactivity
Energy 10MeV
Energy 10MeV
Energy 10MeV
Energy 10MeV

Figure(s)

*Analyzing a test spectrum: Zooming in on a specific area & highlighting a peak*

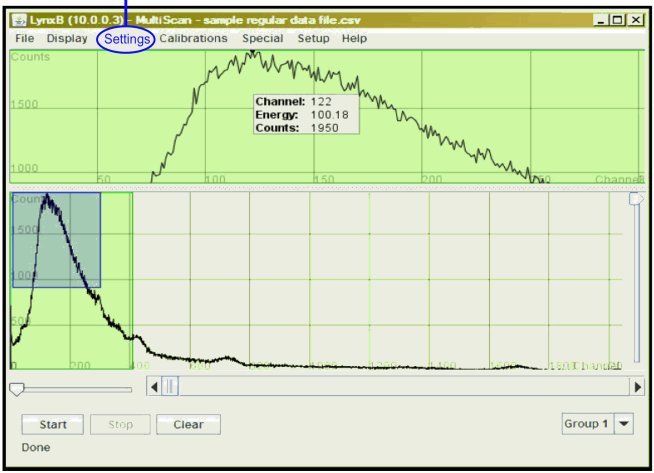


*Checking settings: View & modify settings quickly & easily.*

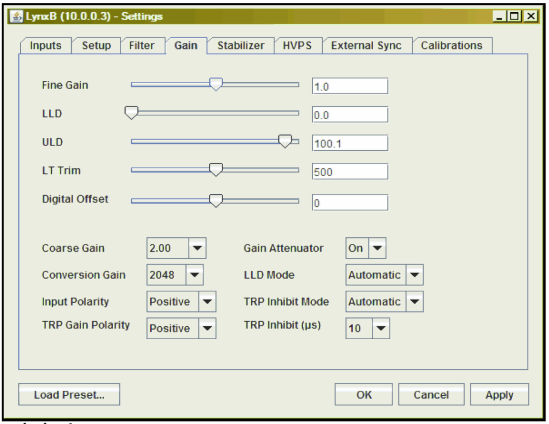


Figure(s) 4

Figure(s) 5

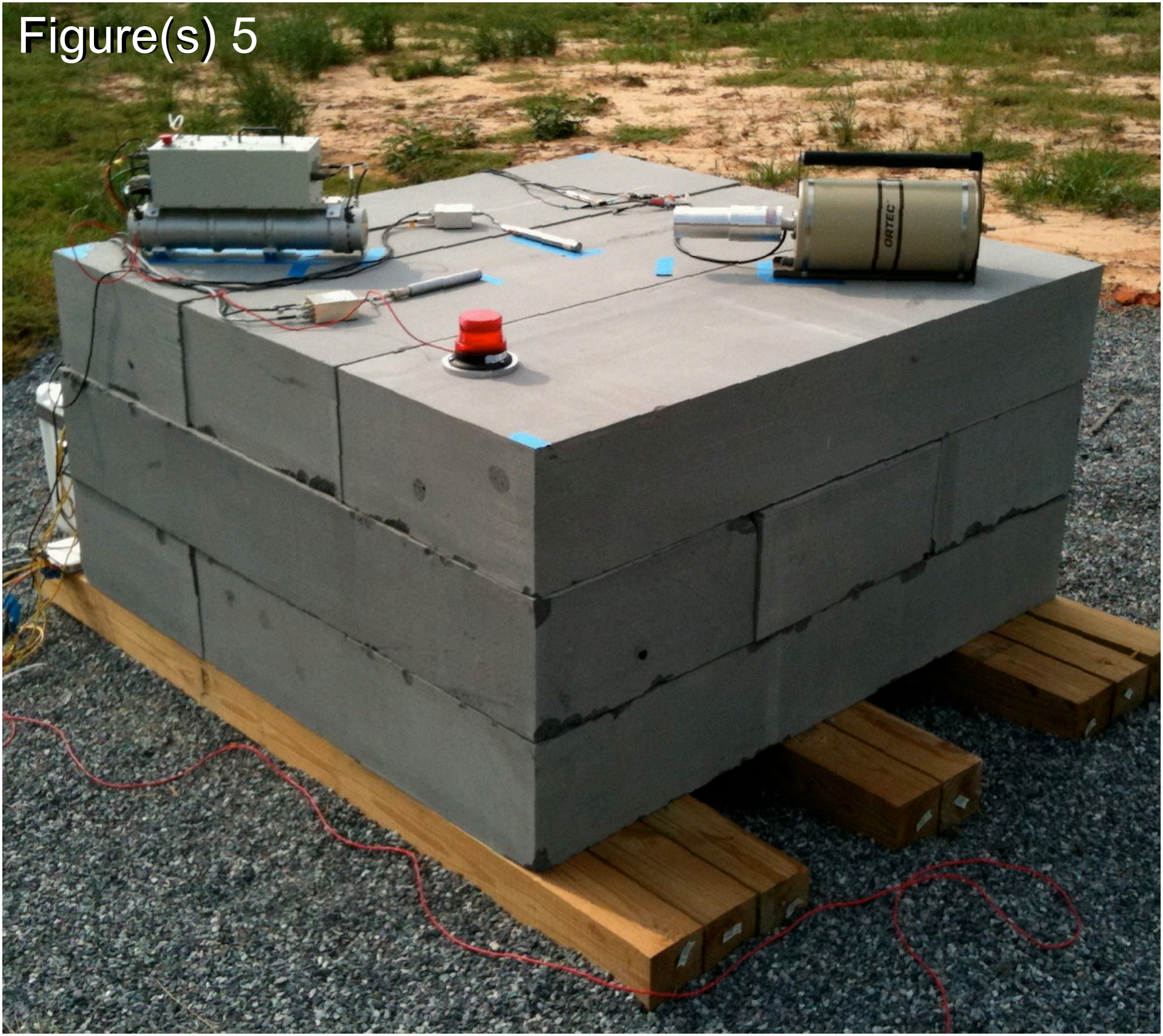

**Figure(s)** 6

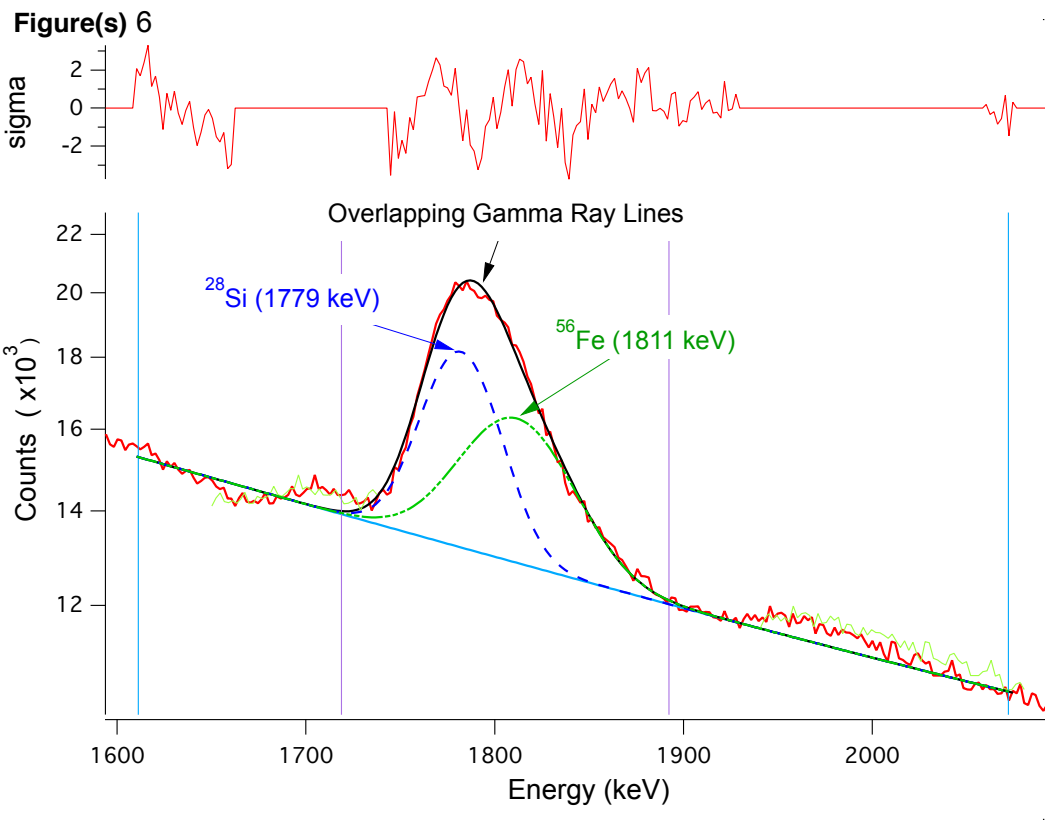
sigma
2
0
-2
Overlapping Gamma Ray Lines
$^{28}$Si (1779 keV)
$^{56}$Fe (1811 keV)
Counts ( x10$^{3}$)
22
20
18
16
14
12
1600
1700
1800
1900
2000
Energy (keV)

Figure(s)

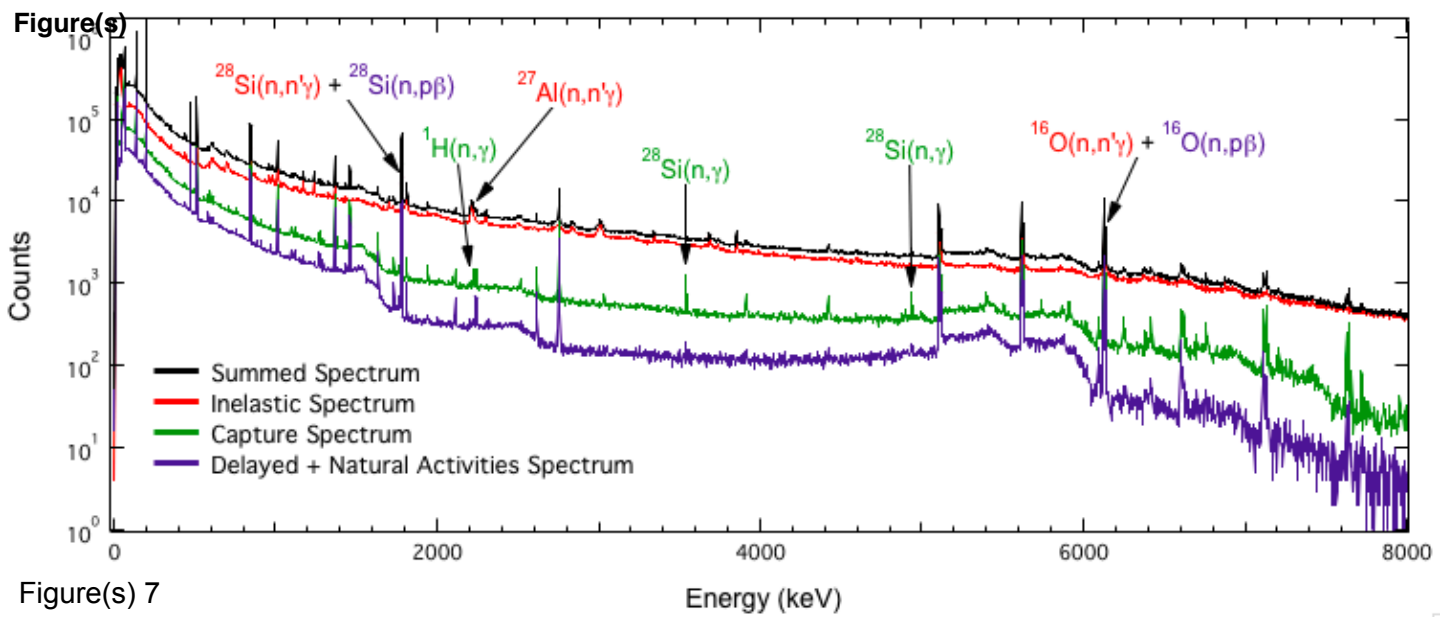


Figure(s) 7

**Figure(s) 8**

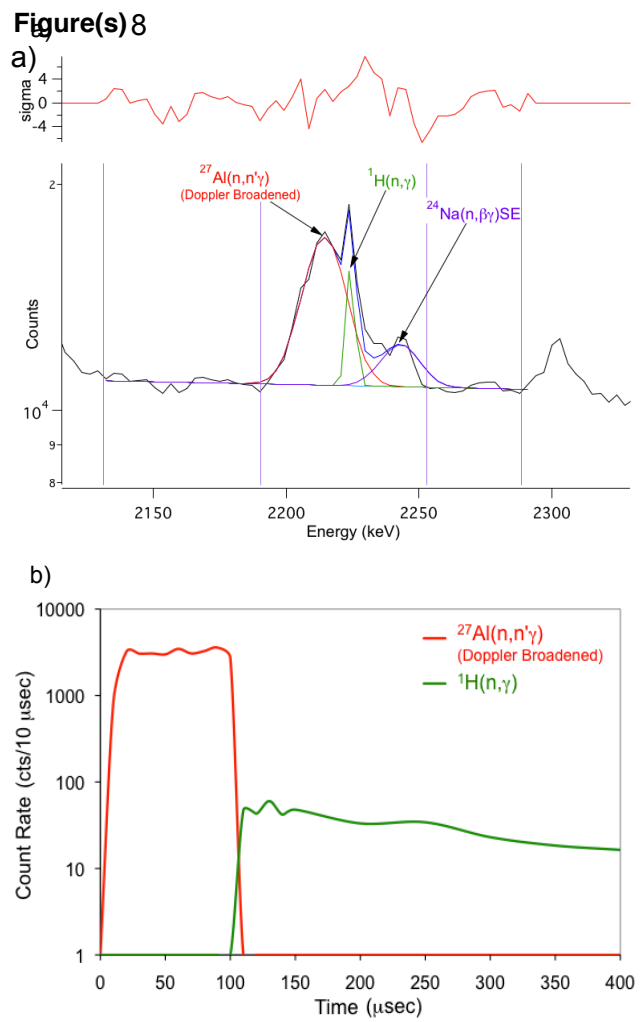
a)
sigma
4
0
-4
$^{27}$Al(n,n'γ)
(Doppler Broadened)
$^{1}$H(n,γ)
$^{24}$Na(n,βγ)SE
Counts
2
$10^4$
9
8
2150
2200
2250
2300
Energy (keV)
b)
10000
1000
100
10
1
Count Rate (cts/10 μsec)
$^{27}$Al(n,n'γ)
(Doppler Broadened)
$^{1}$H(n,γ)
0
50
100
150
200
250
300
350
400
Time (μsec)

**Table(s)**

Table 1. HPGe gamma-ray line intensities ($I_\gamma$) and uncertainties ($\sigma$) for a 6.33-hr PING acquisition on the bare Columbia River basalt monument.

| Energy (keV) | Summed | | Inelastic Scattering | | | Capture – Activation | | |
|---|---|---|---|---|---|---|---|---|
| | $I_\gamma$(cts) | σ(%) | ID | $I_\gamma$(cts) | σ(%) | ID | $I_\gamma$(cts) | σ(%) |
| 1779 | 90480 | 0.48 | $^{28}$Si(n,n'γ) | 31730 | 1.00 | $^{28}$Si(n,pβ) $^{27}$Al(n,γβ) | 57980 | 0.52 |
| 2211 | 24310 | 1.55 | $^{27}$Al(n,n'γ) | 23760 | 1.50 | | | |
| 2223 | 1892 | 16.10 | $^{1}$H(n,γ) | 967 | 14.50 | $^{1}$H(n,γ) | 887 | 7.40 |
| 3539 | 1154 | 8.30 | | | | $^{28}$Si(n,γ) | 1158 | 7.30 |
| 4934 | 1472 | 16.90 | | | | $^{28}$Si(n,γ) | 1151 | 9.21 |
| 6129 | 19920 | 1.10 | $^{16}$O(n,n'γ) | 10900 | 1.67 | $^{16}$O(n,pβ) | 9087 | 1.42 |

**Table(s)**

Table 2: $\gamma$-ray lines to analyze for inelastic $\gamma$-ray spectra time window optimization

| Gamma-Ray Lines (keV) | Possible Sources of Neutron Nuclei Interactions |
|---|---|
| 843 | A, B, C, D, E |
| 1014 | A, D |
| 1779 | F, G, H |
| 1811 | B, C, E |
| 2211 | A |
| 6129 | I, J |

Key:

A: $^{27}Al\ (n, n'\gamma)\ ^{27}Al$

B: $^{56}Fe\ (n, n'\gamma)\ ^{56}Fe$

C: $^{56}Fe\ (n, p)\ ^{56}Mn\ (\beta)\ ^{56}Fe$

D: $^{26}Mg\ (n, \gamma)\ ^{27}Mg\ (\beta)\ ^{27}Al$

E: $^{55}Mn\ (n, \gamma)\ ^{56}Mn\ (\beta)\ ^{56}Fe$

F: $^{28}Si\ (n, n'\gamma)\ ^{28}Si$

G: $^{28}Si\ (n, p)\ ^{28}Al\ (\beta)\ ^{28}Si$

H: $^{27}Al\ (n, \gamma)\ ^{28}Al\ (\beta)\ ^{28}Si$

I: $^{16}O\ (n, n'\gamma)\ ^{16}O$

J: $^{16}O\ (n, p)\ ^{16}N\ (\beta)\ ^{16}O$

**Table(s)**

Table 3. Fast neutron induced count rate and uncertainty for the 6129 keV $^{16}O(n,n'\gamma)$ gamma ray peak for ten time slices during the PNG pulse.

| Time Slice | Time Range (μs) | Count Rate (cts/μs) | Uncertainty (cts/μs) |
|---|---|---|---|
| 1 | 0 - 10 | 9 | ±1 |
| 2 | 10 - 20 | 55 | ±4 |
| 3 | 20 - 30 | 41 | ±3 |
| 4 | 30 - 40 | 42 | ±3 |
| 5 | 40 - 50 | 39 | ±3 |
| 6 | 50 - 60 | 42 | ±3 |
| 7 | 60 - 70 | 41 | ±3 |
| 8 | 70 - 80 | 41 | ±3 |
| 9 | 80 - 90 | 46 | ±3 |
| 10 | 90 - 100 | 45 | ±3 |